HHS Public Access

Author manuscript

Clin Sci (Lond). Author manuscript; available in PMC 2018 August 01.

Published in final edited form as:

Clin Sci (Lond). 2017 August 01; 131(15): 1841–1857. doi:10.1042/CS20170064.

Inhibition of HDAC3 prevents diabetic cardiomyopathy in OVE26 mice via epigenetic regulation of DUSP5-ERK1/2 pathway

Zheng Xu[1,2], **Qian Tong**[1], **Zhiguo Zhang**[1], **Shudong Wang**[1], **Yang Zheng**[1], **Qiuju Liu**[3], **Lingbo Qian**[2,4], **Shao-yu Chen**[5], **Jian Sun**[1,*], and **Lu Cai**[1,2,*]

[1]Cardiovascular Center, the First Hospital of Jilin University, Changchun, 130021 China

[2]Pediatric Research Institute at the Department of Pediatrics, the University of Louisville, Louisville, KY, 40202 USA

[3]Cancer Center, the First Hospital of Jilin University, Changchun, 130021 China

[4]Department of Basic Medical Sciences, Hangzhou Medical College, Hangzhou, 310053 China

[5]Department of Pharmacology and Toxicology, Alcohol Research Center, University of Louisville, Louisville, KY, 40202 USA

Abstract

Inhibition of total histone deacetylases (HDACs) was phenomenally associated with the prevention of diabetic cardiomyopathy (DCM). However, which specific HDAC plays the key role in DCM remains unclear. The present study was designed to determine whether DCM can be prevented by specific inhibition of HDAC3 and to elucidate the mechanisms by which inhibition of HDAC3 prevent DCM. Type 1 diabetes OVE26 and age-matched wild-type mice were given the selective HDAC3 inhibitor RGFP966 or vehicle for 3 months. These mice were then sacrificed immediately or 3 months later for cardiac function and pathological examination. HDAC3 activity was significantly increased in the heart of diabetic mice. Administration of RGFP966 significantly prevented DCM, as evidenced by improved diabetes-induced cardiac dysfunction, hypertrophy and fibrosis, along with diminished cardiac oxidative stress, inflammation, and insulin resistance, not only in the mice sacrificed immediately or 3 months later following the three-month treatment. Furthermore, phosphorylated extracellular signal-regulated kinases (ERK) 1/2, a well-known initiator of cardiac hypertrophy, was significantly increased, while dual specificity phosphatase 5 (DUSP5), an ERK1/2 nuclear phosphatase, was substantially decreased in diabetic hearts. Both of these changes were prevented by RGFP966. Chromatin immunoprecipitation assay showed that HDAC3 inhibition elevated histone H3 acetylation on the *DUSP5* gene promoter at both two-time

Corresponding authors: Dr. Jian Sun, Cardiovascular Center, the First Hospital of Jilin University, 71 Xinmin Street, Changchun, China. sunjianemail@126.com; Phone number: +8613844038776, Dr. Lu Cai, Pediatric Research Institute, University of Louisville, 570 S. Preston Street, Baxter I, Suite 304F, Louisville, KY 40202, USA. lu.cai@lousiville.edu; Phone number: 15025921056.

AUTHOR CONTRIBUTION

Jian Sun, Qian Tong, Zhiguo Zhang, Yang Zheng, Qiuju Liu and Lu Cai contributed to the initial experimental discussion and designs. Jian Sun and Lu Cai consistently directly guided the research project progression. Zheng Xu set up the animal model, analyzed the data and wrote the manuscript. Zheng Xu, Shudong Wang, Xiaozhen Dai, and Lingbo Qian performed experiments. Jian Sun, Shao-yu Chen, and Lu Cai wrote or revised the manuscript. All authors have reviewed the final manuscript and approved the submission to this journal.

COMPETING INTERESTS

The authors declare no conflicts of interest.

points. These findings suggest that diabetes-activated HDAC3 inhibits DUSP5 expression through deacetylating histone H3 on the primer region of *DUSP5* gene, leading to the derepression of ERK1/2 and the initiation of DCM. This study indicates the potential application of HDAC3 inhibitor for the prevention of DCM.

Keywords

Diabetic cardiomyopathy; Epigenetic regulation; ERK1/2; DUSP5; HDAC3 inhibition

Introduction

Diabetes mellitus is a global health problem, as evidenced by the facts that the number of global diabetic patients has been up to 415 million in 2015 and that from 2012 to 2015, diabetes and its complications has resulted in approximately 1.5 to 5.0 million deaths each year (1). In terms of cardiac complications, diabetes leads to cardiac vascular injury, the formation of atherosclerotic plaque, and even myocardial infarction. Among these complications, a myocardial disorder without coronary artery disease and hypertension, named as diabetic cardiomyopathy (DCM), has received much attention in recent years (2). DCM has been noticed in both human and animal models with type 1 or type 2 diabetes (3). In diabetic mouse models which were generated by either streptozotocin (STZ) or transgenic approach, mice displayed decreased cardiac diastolic and/or systolic dysfunction and a variety of morphological changes, including cardiac hypertrophy and interstitial fibrosis (4–6). Some mechanisms have been proposed for contributing to the pathogenesis of DCM (7–9), including the alterations in ion homeostasis, especially calcium transients, mitochondrial dysfunction, accumulation of advanced glycated end-products, accumulation of toxic lipids, trace metal dyshomeostasis, and hyperlipidemia and inflammatory cytokines. In the clinic, patients who were randomized initially to the more intensified insulin regimen and then returned to regular glycemic control continued to have better prevention of various microvascular and macrovascular events comparing with those who were only regular glycemic control. This phenomenon was coined as “metabolic memory” (10, 11) and recently was attributed to epigenetic modifications (11, 12).

Histone deacetylases (HDACs), a class of epigenetic modification enzymes, remove acetyl groups (O=C-CH3) from a ε-N-acetyl lysine amino acid on a histone, making the DNA chain to twine the histones more tightly, and resulting in inhibition of gene expression. The 18 HDACs are encoded by distinct genes and are divided into four classes. Class I, II, and IV HDACs are zinc-dependent enzymes, whereas class III HDACs, which are also known as sirtuins, require nicotinamide adenine dinucleotide (NAD^+) for catalytic activity (13). Recent studies have shown that activation of HDACs was associated with DCM since total HDAC inhibition attenuated diabetes-induced cardiac injury in the STZ-induced diabetic animal models (14, 15). In these two studies, it is unclear which specific HDAC really involves in the pathogenesis of DCM because they only used non-specific HDAC inhibitor to inhibit total HDAC activity.

Several previous studies reveal that extracellular signal-regulated kinases (ERK) 1/2 are involved in the development of cardiac hypertrophy and interstitial fibrosis (16, 17). For instance, Ferguson et al. found that class I HDAC inhibition repressed cardiac hypertrophy induced by several pathological insults in vitro via inhibition of ERK1/2 by Dual Specificity Phosphatase 5 (DUSP5) (18). Furthermore, HDAC3 was reportedly involved in different aspects of heart pathologic change, including heart failure (19), hypertrophy (20) and abnormal energy metabolism (21), but so far no information is available for its role in DCM.

In the present study, therefore, we tested our hypothesis that specific inhibition of HDAC3 with HDAC3 selective inhibitor, RGFP966, may prevent the development of DCM with OVE26 mice that spontaneously develop type 1 diabetes. We also explored whether its cardioprotection from diabetes is mediated by stimulating DUSP5 to inactive ERK1/2 signaling pathway. In addition, considering the existence of metabolic memory due to epigenetic modification for the development of diabetic cardiovascular complications, we treated diabetic mice for the first 3 months and then observed the treatment effect immediately and 3 months later after the end of 3-month treatment to explore the existence of “cardiac protective memory”.

Material and methods

Animals

Male OVE26 and wild-type (WT) FVB mice were housed at the University of Louisville Research Resources Center with a 12-h light/dark cycle at 22°C. All animal experimental procedures were approved by the Institutional Animal Care and Use Committee of the University of Louisville, and were performed complying with the Guide for the Care and Use of Laboratory Animals published by the US National Institutes of Health (NIH Publication No. 85-23, revised 1996).

The specific HDAC3 inhibitor RGFP966 (10 mg/kg, Abcam, Cambridge, MA, USA) and pan-HDAC inhibitor valproic acid (VPA, 200 mg/kg, Santa Cruz, Dallas, TX, USA) were subcutaneously injected into the mice every other day for 3 months (22). The specific HDAC inhibitor RGFP966 was dissolved in DMSO and diluted in 30% hydroxypropyl beta-cyclodextrin and the final DMSO concentration was no more than 1%. VPA was dissolved in phosphate buffer solution. In the present study, VPA was included as a total HDAC inhibition control. Cardiac protection from DCM will be compared between HDAC total inhibition of VPA and HDAC3 specific inhibition with RGP966 in order to define the contribution of HDAC3 to HDAC total inhibition-mediated cardiac protection from DCM.

Animals were divided into six experimental groups: WT + vehicle, WT + RGFP966, WT + VPA, OVE + vehicle, OVE + RGFP966, and OVE + VPA. At the end of the 3-month treatment, five to seven mice from each group were sacrificed as the time point of 3 months (labeled as 3 M) cohort. The remaining animals (n= 5 at least) in each group were kept for another 3 months without HDAC inhibitors’ treatment (labeled as 6 M). Mice were intraperitoneally anesthetized with Avertin (tribromoethanol, 350 mg/kg). The chest cavity was opened, and heart was removed for weighing, and then derived into three pieces. One

piece was for protein and RNA analysis, one for frozen section and the rest was fixed in 10% neutral buffered formalin for histological analysis.

Echocardiography

Echocardiography was performed as we described previously (23). In brief, heart rate (HR), parasternal long-axis and short-axis views in mice anesthetized with isoflurane were recorded by transthoracic echocardiography (Vevo 770, Visual Sonics, Canada) equipped with a high-frequency ultrasound probe (RMV-707B). Left ventricular (LV) dimensions and wall thicknesses were assessed on the base of parasternal short axis M-mode images. Ejection fraction (EF), fractional shortening (FS), LV mass, and LV end volume were instantaneously computed by Vevo770 software (Table 1).

Histology and immunostaining

Mice were anesthetized and the hearts were collected, fixed in 10% formalin, dehydrated in graded alcohol series, cleared with xylene, embedded in paraffin and sectioned at 5 μm thickness. FITC-conjugated WGA staining (Alexa Fluor-488, Invitrogen, Carlsbad, CA, USA) was performed to evaluate the cardiomyocyte size under the confocal microscope. Sirius-red staining was performed to detect collagen deposition in cardiac tissues (23).

To assess the production of reactive oxygen species (ROS), frozen heart tissue segments were cut into 8 μm sections in a cryostat and placed on a microslide. Sections were washed in phosphate buffer saline (PBS) for 3 times (5 min/time) at 37°C. After incubated for 1 h at 37°C with 10 μM dihydroethidium (DHE) (Thermo Fisher, Grand Island, NY, USA), fluorescence was detected using a 585-nm filter with fluorescence microscopy (XI 71 Olympus, Tokyo, Japan). Fluorescence intensity was analyzed by the use of ImageJ software.

Determination of HDAC activity

HDAC and HDAC3 activities were determined using HDAC Activity Fluorometric Assay Kit (K330-100 and K343-100, BioVision, CA, USA) based on the protocol provided by the manufacturer. Forty μg protein lysate was diluted to 85 μl (final volume) of ddH_2O in each well along with a well of ddH_2O only as the background. HDAC Assay Buffer (10 μl of 10X) and 5 μl of the HDAC fluorometric substrate were added to each well with thoroughly mixing. Then, the plates were incubated at 37°C for 1 h before adding 10 μl of Lysine Developer to stop the reaction. The plate was incubated at 37°C for another 30 min. All the reacted samples were analyzed in the fluorescence plate reader at Ex/Em = 350/450 nm. The Histone Deacetylase activity can be expressed as the relative fluorescence units per μg protein. For the measurement of HDAC3 activity, first, the standard curve was prepared by following the protocol in HDAC3 Activity Fluorometric Assay Kit. In details, 10 μM AFC (7-amino-4-trifluoromethyl coumarin) at 0, 1, 2, 4, 6, 8 and 10 μl was added to individual wells in a 96-well plate and adjust the volume to 100 μl/well with HDAC3 assay buffer to generate 0, 10, 20, 40, 60, 80, 100 pmol/well of AFC standard. Read fluorometrically at Em/Ex = 380/500 nm after mixing. Then, for sample preparations, samples were prepared as replicates o f u p t o 2 5 μ l/well w ith H DAC3 Assay Buffer i n a 9 6-well plate. One sample replicate added 2 μl HDAC3 Inhibitor (Trichostatin A) was used as background

control. After mix well and incubate for 10 min at 37°C, 25 μl substrate solution (23 μl HDAC3 Assay Buffer and 2 μl HDAC3 Substrate) was added into each test sample and background control wells except Standard Curve wells and mix well, then incubated at 37°C for 30 min. After then, 10 μl of Developer and 40 μl HDAC3 Assay Buffer were added to each well and incubated another 5 min at 37°C. The plates were read in the fluorescence plate reader at Ex/Em = 380/500 nm for each background well (RB) and sample well (RS), respectively. The RFU of fluorescence generated is Δ RFU = RS – RB. Apply the Δ RFU to the standard curve to get B pmol of AFC. At last the final HDAC3 activity was calculated by the following formula:

$$\mathbf{HDAC3\ Activity}=(\mathbf{B}\times\mathbf{Sample\ Dilution\ Factor})/(\mathbf{30}\times\mathbf{V})=\mathbf{pmol/min/ml}=\mathbf{U/ml}.$$

B is the AFC amount from the Standard Curve (in pmol); 30 is the sample/substrate incubation time (in min); V is the sample volume added into the reaction well (in ml). One unit is defined as the amount of HDAC3 able to generate 1.0 pmol of AFC per minute at 37°C when incubated with the HDAC3 Substrate (R-H-K-K(Ac)-AFC).

Determination of lipid peroxidation accumulation

The lipid peroxidation accumulation in the hearts was evaluated by the content of malondialdehyde (MDA) as described previously (24).

Preparation of nuclear protein

As described in our previous study (23), nuclear extracts were purified with the nuclear extraction kit (Abcam, Cambridge, MA, USA).

Western blot assay

Western blot was carried out as we detailed previously (23). Primary antibodies used for this assay include atrial natriuretic peptide (ANP), connective tissue growth factor (CTGF), GAPDH, Lamin B1, DUSP5, Histone H3 and β-actin (Santa Cruz Biotechnology, Dallas, TX, USA), 3-nitrotyrosine (3-NT), acetyl-Histone H3 (Millipore, Billerica, CA), 4-hydroxy-2-nonenal (4-HNE, Alpha Diagnostic International, San Antonio, TX, USA), phosphorylated c-Jun N-terminal protein kinase (p-JNK), tumor necrosis factor alpha (TNF-α), glucose transporter type 1 and 4 (GLUT1 and GLUT4) (Abcam, Cambridge, MA, USA), p-ERK1/2, ERK1/2, JNK, p-p38, p38, insulin receptor substrate 1 (IRS1), p-Akt, Akt, 5' AMP-activated protein kinase alpha (AMPKα), p-AMPKα, HDAC3 and acetyl-Histone H3 (Lys9/Lys14) (Cell Signaling Technology, Danvers, MA, USA), and plasminogen activator inhibitor-1 (PAI-1, BD Bioscience, San Jose, CA, USA). The protein blot on the nitrocellulose membrane was captured by the ChemiDoc Touch Imaging System (Bio-Rad, Hercules, CA, USA) and was normalized to that of GAPDH or β-actin.

RNA purification, reverse transcription and quantitative PCR (qPCR)

TRIzol Reagent (Invitrogen, Carlsbad, CA, USA) was used to purify the total RNA from heart tissues. RTq-PCR was performed as previously described (23). Primers [ANP: Mm01256744_m1; collagen I: Mm01302043_g1; fibronectin-1 (FN-1): Mm01255747_g1;

DUSP5: Mm01266106; GAPDH: Mm99999915_g1] for PCR were obtained from Thermo Fisher (Grand Island, NY, USA).

Chromatin immunoprecipitation (ChIP) assay

As described in our previous study (25), EpiQuik™ Tissue ChIP Kit (P-2012; Epigentek Group Inc., Farmingdale, NY, USA) was used to perform the ChIP assay according to the manufacturer's protocol. In brief, the acetylated histone H3 antibody (1 μg, Epigentek Group Inc.) or 1 μl of normal mouse IgG (as a negative control) was used to pre-coat the assay wells. Meanwhile, 30 mg of heart tissue was cut into little pieces and cross-linked with 1% formaldehyde. The cross-link was stopped by glycine solution (1.25 M). After tissue disaggregation and the nuclei isolation, the DNA was sheared by sonication (S-450-Dwithmicro-tip probe; Emerson Industrial, St. Louis, MO, USA) with 5 pulses of 20 s each separated by 40 s rest on ice (output control: 2). After centrifugation, 5 μl of the diluted supernatants were used as input DNA. The other diluted supernatant (100 μl) was added to the acetylated histone H3 antibody-coated wells followed by incubation at room temperature for 60 min. ChIP-enriched DNA fragments were precipitated, purified, and assayed by quantitative PCR with the following primers: DUSP5 forward 5' CTGACACTCCACCGGTAGTC 3', reverse 5' GGGCGTCTTAGAGCGAGAAA 3'. The value was computed relative to a calibrator ($2^{-\Delta\Delta Ct}$) and normalized to the input.

Statistical analysis

Data were expressed as means ± SD (n=5–7 per group). One-way ANOVA followed by post-hoc pairwise repetitive comparisons with Turkey test was used for data comparison among groups. Statistical analysis was performed with Origin 8.0 Lab data analysis and graphing software. P values less than 0.05 were considered to be statistically significant.

Results

General features and cardiac HDAC activity in the mouse

We first examined the general features of WT and OVE26 mice treated with vehicle, VPA or RGFP966. Before the treatment, the baseline cardiac function measured by echocardiography showed no significant difference between OVE26 and WT mice at 2 months of age (Fig. 1A). The peripheral blood glucose concentration was measured every four weeks with collecting blood from the tail tip vein. Quintessentially, mice with blood glucose readings of >250 mg/dl were diagnosed diabetic. In this project, the blood glucose of diabetic mice was more than 400 mg/dl, indicating the presence of diabetes. Three months treatment with RGFP966 or VPA did not significantly affect the blood glucose levels in both OVE26 and WT mice (Fig. 1B). Next, the activity of HDAC3 and HDAC was measured, showing that in OVE26 mice activity of both HDAC3 and HDAC was significantly increased compared with WT mice at the 3 M time point, which persisted to the 6 M time point. Treatment with either RGFP966 or VPA for 3 months significantly reduced the diabetes-up-regulated HDAC3 and HDAC activities, even at 6 M time point (Fig. 1C, D). In addition, the acetylated histone H3, especially at Lysine 9/14 (Fig 1E–G), was increased in RGFP966 and VPA-treated group at two-time points, which confirmed that the increased acetylated histone H3 induced by inhibiting HDAC could persist 3 months after cessation of

HDAC inhibitor therapy although the increased levels were reduced at 6 M than those at 3 M.

RGFP966 prevented diabetes-induced cardiac dysfunction and pathological changes in the OVE26 mouse

To define whether HDAC3 inhibition by RGFP966 protected against diabetes-induced cardiac dysfunction in OVE26 mice, we examined cardiac function with echocardiography and found that OVE26 mice had significantly increased LV internal diastolic diameter (LVID; d), LV internal systolic diameter (LVID; s), LV end-diastolic volume (LV vol; d), LV end systolic volume (LV vol; s), LV mass, and decreased EF and FS compared with WT mice (Table 1). Three-month treatment with RGFP966 improved these cardiac functional parameters in diabetic mice, which lasted to the 6 M time point. There was no significant difference between RGFP966 and VPA treatment groups in terms of cardiac function improvement.

We next determined the structural changes after HDAC3 inhibition. Compared with WT mice, OVE26 mice exhibited a higher heart weight to tibia length ratio (Fig. 2A) and enlarged cardiomyocyte size as determined by FITC-conjugated wheat germ agglutinin (WGA) staining (Fig. 2B, C). The mRNA and protein expression of ANP, a cardiac disease marker, was also increased in the OVE26 mouse heart (Fig. 2D–F) at both 3 M and 6 M time points. However, all these cardiac hypertrophic changes were significantly ameliorated by the treatment of RGFP966, which still sustained until 3 months after the end of 3-month treatment. There was no significant difference between RGFP966 and VPA treatment groups in terms of cardiac hypertrophy improvement.

Compared to WT mice, OVE26 mice exhibited increased fibrosis as revealed by the Sirius-red staining (Fig. 3A, B), which was supported by the increased expression of collagen I and FN-1 (Fig. 3C, D). Evidence of cardiac fibrosis was further consolidated by the changes in the expression of the pro-fibrotic mediator, CTGF and FN-1 as determined by Western blot (Fig. 3E–G). RGFP966 treatment decreased the collagen accumulation and the expression of CTGF and FN-1 in the diabetic heart. There was no significant difference between RGFP966 and VPA treatment groups in terms of cardiac fibrosis improvement. Collectively, these findings suggest that 3-month administration of RGFP966 significantly prevents the diabetes-related cardiac remodeling at both 3 M and 6 M time points.

RGFP966 inhibited diabetes-induced oxidative stress and inflammation in the OVE26 mouse heart

Oxidative stress and inflammation play important roles in diabetes-induced cardiac pathogenesis. Consistent with this notion, ROS production, detected by staining with DHE (a superoxide indicator, Fig 4A, B) and lipid peroxidation, reflected by MDA contents (Fig. 4C), were increased in the heart of OVE26 diabetic mice, but not significantly in VPA- or RGFp966-treated OVE26 diabetic mice, compared with that of in the WT heart. Furthermore, Western blot of 4-HNE (Fig. 4D, E) and 3-NT (Fig. 4F, G) as oxidative and nitrative proteins, respectively, were significantly increased in OVE26 diabetic mice, which was significantly reduced by RGFP966 at both 3 M and 6 M time points. Similarly, the

expressions of inflammatory factors PAI-1 and TNF-α (Fig. 5A–C) were also substantially increased in the OVE26 diabetic heart compared with that of in the WT heart, which were suppressed in the RGFP966 treated diabetic mouse at 3 M and 6 M time points. There was no significant difference between RGFP966 and VPA treatment groups in terms of cardiac oxidative stress and inflammation improvement.

RGFP966 improved insulin receptor signaling pathway in the OVE26 mouse heart

Insulin resistance also plays an important role in the type 1 diabetes disease process that is commonly recognized (26). We checked whether the insulin receptor signaling pathway is reduced in OVE26 mice and improved by the treatment of HDAC inhibition. As shown in Fig 6, HDAC3 inhibitor reversed the diabetes-induced classical insulin pathway suppression, including the upregulation of IRS1 expression, p-Akt to total Akt ratio, and GLUT4 expression (Fig 6A–F), as did VPA, at both two-time points. Interestingly, the expression of GLUT1 was not affected by the treatment of HDAC inhibitors in the OVE26 diabetic mouse heart (Fig 6G, H).

It is reported that AMPK is associated with the process of glucose metabolism in the high fat diet-fed diabetic mice (27). In the OVE26 diabetic mouse model, we also found that p-AMPKα decreased in the diabetic heart, which was reversed by the treatment of RGFP966 and VPA at both two-time points without difference between two kinds of inhibitors (Supplementary Fig 1A, B).

RGFP966 blocked the activation of ERK1/2 in nucleus by epigenetic regulation of DUSP5 via histone H3 acetylation in the OVE26 mouse heart

Previous studies have shown a connection between DCM and the mitogen-activated protein kinase (MAPK) pathway (28), so we decided to examine whether HDAC3 inhibitor could block the activation of major MAPK family members: ERK1/2, JNK, and p38 MAPK. As shown in Fig 7 and Supplementary Fig 1, phosphorylated ERK1/2, JNK and p38 MAPK protein levels were significantly increased in the hearts of OVE26 diabetic mice compared with those of WT hearts at both 3 M and 6 M time points. RGFP966 treatment blocked the activation of cardiac ERK1/2 (Fig 7A, B), but not JNK or p38 MAPK in OVE26 diabetic mice (Supplement Fig. 1A–C). These inhibitory effects imposed by RGFP966 persisted for another 3 months after termination of treatment. There was no significant difference between RGFP966 and VPA treatment groups in terms of the MAPK expression.

A previous study showed that increased nuclear ERK1/2 signaling was linked to the development of cardiac hypertrophy (18). Therefore, we further examined the expression levels of ERK1/2 in the nucleus by Western blot. Indeed, the increased expression of nuclear ERK1/2 in the OVE26 diabetic mouse heart was observed, which was suppressed by RGFP966 (Fig. 7C, D). As a nuclear ERK1/2 phosphatase, DUSP5 specifically dephosphorylates and inactivates ERK1/2 in the nucleus (29). To address whether HDAC3 inhibitor could stimulate DUSP5 expression in the diabetic mouse heart, the DUSP5 expression was investigated at both mRNA and protein levels. The DUSP5 expression in the OVE26 mouse heart was inhibited at both 3 M and 6 M time points, which was reversed by the treatment of RGFP966 (Fig. 7E–G). Next, to further understand how the HDAC3

inhibitor increased the expression of DUSP5 in the diabetic mouse heart, we performed ChIP assay with an acetylated histone H3 antibody to determine the transcriptional management of DUSP5 in chromatin. We found that RGFP966 increased the acetylated level of histone H3 on the cardiac *DUSP5* gene promoter compared with the OVE26 diabetic group at both 3 M and 6 M time points (Fig. 7H). There was no significant difference between RGFP966 and VPA treatment groups with regard to the expression of nuclear ERK1/2, DUSP5, and acetylated histone H3.

Discussion

A few studies have shown the association of total HDAC inhibition with DCM, which is substantially advanced by the present work in the following aspects: (1) We are the first study to specifically define the pivotal role of HDAC3 inhibition in the prevention of DCM; (2) Both previous two studies have used STZ-induced type 1 diabetes model that may involve in the STZ's effect on the total HDAC activity. Here we have used well-appreciated genetically OVE26 spontaneous type 1 and its potential epigenetic cardioprotection against DCM in the type 1 diabetic mice; (3) There was no significant difference between HDAC inhibition and HDAC3 inhibition groups in terms of cardiac function and pathology improvement in the OVE26 diabetic mouse, which suggests the predominant role of HDAC3 in the development of DCM; (4) Mechanistically, the most important protection by HDAC3 inhibition against DCM probably is mediated by its suppression of diabetes-induced activation of ERK1/2 in the nucleus, but not that of JNK and p38 MAPK, and also increases in the expression of DUSP5, a nuclear ERK1/2-specific phosphatase and the acetylation of histone H3 on the promoter region of *DUSP5* gene. All these results indicate the crucial role for HDAC3 in the development of DCM.

As epigenetic regulators, HDACs catalyze the removal of acetyl groups from lysine residues in a variety of proteins. Classically HDACs deacetylate nucleosome histones and alter the electrostatic properties of chromatin in a manner that represses gene expression (30, 31). Inhibition of HDACs using small molecules such as butyrate, VPA or trichostatin A exerts multiple cardioprotective effects, such as the anti-hypertrophy (32, 33), anti-fibrosis (34, 35), anti-oxidative stress (36), anti-inflammation (37, 38), and anti-apoptosis (39) under non-diabetic conditions, and also anti-DCM (14, 15). Although HDACs are the promising therapeutic target for multiple cardiovascular diseases, the diversity of HDAC isoforms constrain the practice. It is urgently needed to clarify the association of specific HDAC and disease, and to develop HDAC inhibitors with high specificity and selectivity in order to reduce unwanted off-target effects.

In the present study, we used RGFP966, an HDAC3 inhibitor (40), to examine the epigenetic effect of HDAC3 on DCM. In addition, VPA was used as the total HDACs inhibitor to detect the cardioprotection in the OVE26 type 1 diabetes mice too. Although butyrate was used in the previous studies as total HDAC inhibitor (15), pharmacokinetic studies have confirmed its lower cardiac distribution, compared to VPA (41, 42). In addition, phase II/III clinical trials have confirmed that VPA is a safe medicine for the therapy some cancers (43, 44). More importantly, VPA is also an established drug for the long-term therapy of epilepsy because of its HDAC inhibition activity (45). Up to date, a number of studies have shown

that VPA plays an important role in the prevention of multiple cardiac pathological changes induced by different stimuli (36, 46–48), including type 2 diabetes (49).

As shown in the results, HDAC3 specific inhibitor RGFP966 did not affect the blood glucose levels, but inhibited the activity of HDAC3 and preserved cardiac function in diabetic mice. Meanwhile, RGFP966 prevented the major pathological manifestations including cardiac hypertrophy as evidenced by decreased expression of hypertrophic markers, the heart weight to tibia length ratio, and cardiomyocyte size. It also significantly diminished the cardiac fibrosis in diabetic mice as evidenced by reduced expression of the fibrosis markers and collagen accumulation. Pan-HDAC inhibitor VPA similarly diminished cardiac injuries induced by diabetes as HDAC3 specific inhibitor RGFP966. Together, HDAC3 inhibition could protect the heart from the injury induced by diabetes in different perspectives.

Ferguson et al. found that Trichostatin A, a non-selective HDAC inhibitor, suppressed the ERK1/2 phosphorylation induced by different stimuli (18). A prior study revealed that HDAC3 governed the TGF-β-induced phosphorylation of ERK1/2 in C3H10T1/2 cells (50). In the present study, we found that HDAC3 inhibitor RGFP966 not only decreased the cardiac nuclear ERK1/2 but also reduced DCM in the OVE26 type 1 diabetes mice, which indicates that down-regulation of cardiac nuclear ERK1/2 might be a key mechanism of hampering DCM by HDAC3 inhibitor on the basis of the argument that nuclear ERK1/2 signaling plays a major role in pathological cardiac hypertrophy (51, 52) and the development of DCM (16, 53).

As a nuclear ERK1/2 specific phosphatase, DUSP5 dephosphorylates the activated ERK1/2 and inhibits the hypertrophic signaling pathway induced by phosphorylated ERK1/2. Meanwhile, based on the study of Ferguson and his group, the MEK-ERK signaling promotes class I HDAC-mediated suppression of DUSP5 expression, thereby providing a self-reinforcing mechanism to sustain ERK1/2 signaling in response to stress stimuli (18). Our results showed that the expression of DUSP5 was decreased in the diabetic heart, which was prevented by RGFP966. Mechanistically, this prevention was achieved potentially through enhancing histone H3 acetylation on the *DUSP5* gene promoter region. HDAC3 specific inhibitor RGFP966 similarly diminished nuclear ERK1/2 expression, up-regulated DUSP5 and histone H3 acetylation in the OVE26 diabetic heart as did Pan-HDAC inhibitor VPA. These results indicate that epigenetic regulation of the DUSP5-ERK1/2 pathway via inhibiting HDAC3 might be the key component for HDAC-target therapy for DCM.

The most impressive feature in this study was that we set up two-time points to evaluate the protective effects of the HDAC3 inhibitor on DCM mice, in which mice were treated with the agent for 3 months followed by non-treatment for another 3 months. The inspiration of this setup came from the “metabolic memory” phenomenon that associated with epigenetics (10, 11). We found that the activity of both HDAC3 and total HDAC are increased in the heart of diabetic mice. These diabetes-induced cardiac damages were significantly inhibited for the first 3 months by treatment with RGFP966 or VPA, which sustained for another 3 months after the end of 3-month treatment. Such phenomenon is called as “cardiac protective memory”, which is similar to “metabolic memory”, observed in previous studies

for diabetic patients with intensified glycemic control (10, 11). In the current work, the level of acetylated histone H3 on the *DUSP5* gene promoter region was still elevated by the HDAC3 inhibitor at 6 M time point, which might contribute to the maintenance of ERK1/2 inactivation even during the withdrawal period and produce the “cardiac protective memory” by epigenetic up-regulation of DUSP5.

As shown in Fig 6, however, HDAC3 inhibitor reversed diabetes-induced classical insulin resistance in the heart, shown by upregulating IRS1 expression, Akt phosphorylation, and GLUT4 expressions, as does VPA, at both two-time points. These results are consistent with previous studies on the effect by HDAC inhibition on insulin resistance in different models (54–56), including in the heart of diabetic mice (15, 57, 58). Therefore, reducing insulin resistance may contribute, at certain levels, to the cardioprotection of HDAC3 inhibitor in OVE26 diabetic mouse model although the exact mechanism needs to be further explored in our future work. Here what calls for special attention is that the lowering blood glucose was not found although previous studies indicated that HDAC inhibitors could reduce blood glucose through improving insulin resistance related signaling pathway. In a low-dose-STZ and high fat diet-induced type 2 diabetic mouse model, HDAC inhibition could reduce blood glucose through improving the insulin receptor signal pathway (57). In a STZ-induced type 1 diabetic mouse model (single dose of STZ at 200 mg/kg) a complete elimination of pancreatic β cell model that is similar to what we used OVE26 mice (59), HDAC inhibition didn’t decreased blood glucose although it reversed the reduction of cardiac GLUT1 and GLUT4 induced by diabetes (15), a similar pattern as what we show in OVE26 mice (Fig. 1B, Fig. 6). Interestingly, HDAC inhibition could reduce the blood glucose slightly in STZ-induced diabetic rat model where a single dose of STZ at 60 and 65 mg/kg, respectively, was given (14, 56). Therefore, in multiple low doses of STZ-induced diabetic mouse model, and a single dose of STZ-induced diabetic rat model, pancreatic β cells may not have been completed destroyed, which were probably rescued by inhibition of HADCs in certain unknown reasons, resulting in certain small amount of insulin to reduce blood glucose. For this discrepancy, we will further explore in the future studies.

For the result of GLUT4 expression, we only examined the change in the heart, which partly consistent with the study mentioned above (15), but didn’t know whether GLUT4 was upregulated in other organs. Therefore, based on our own results and a previous work (15), we may conclude that, even though the extent of the cardiac IRS1-Akt-GLUT4 change were improved in certain extends, it remains not enough to reduce blood glucose in the severe type 1 diabetic models without insulin level improvement (OVE26 mice and one single large dose of STZ-induced mode).

Several studies revealed the activation of AMPK related signaling pathway with non-specific HDAC inhibitors, MPT0E014 and VPA, in both type 1 diabetic rats and obese mice with several other metabolic variables (58, 60). However, the effect of the HDAC3 inhibitor on AMPK in the diabetic heart remains unclear. As shown in Supplemental Fig A, we found that AMPKα phosphorylation was decreased in the diabetic heart but not significantly in the heart of diabetic mice treated with both HDAC inhibitors VPA and RGFP966. However, whether activation of AMPK-mediated metabolism by inhibition of HDACs or HDAC3

contributes to the cardiac protection from DCM remains unclear and will be further explored in the future.

There remain a few limitations in the present study. For example, we did not perform the exmination for insulin resistance regrettably although we provide the result of insulin signaling pathway. In addition, we did not further confirm the findings in the cardiac specific ERK1/2 knockout mouse, which is not available for the time being. We did not directly define the pivotal role of ERK1/2 in the development of DCM though nuclear ERK1/2 activity was previously reported to modulate cardiac hypotrophy in other heart disease models (18). The more detailed mechanisms on how HDAC3 mediates the expression of DUSP5 also remains to be explored in the future.

In summary, our study reveals for the first time that HDAC3 inhibition by RGFP966 prevents diabetes-induced cardiac dysfunction and remodeling in the OVE26 diabetic mice. The cardiac protection by inhibition of HDAC3 from DCM is persistent at least for 3 months after the end of treatment, like a “protective memory” phenomenon. Mechanistically, this cardioprotection of HDAC3 inhibition may be mainly mediated by the epigenetic regulation of DUSP5-ERK1/2 pathway via acetylating of histone H3 on the DUSP5 gene promoter. However, we are also aware that HDAC3 inhibition-mediated stimulation of insulin intracellular sigalings and the activation of AMPK may also have certain contributions. This study suggests the potential application of HDAC3 inhibitor for the prevention of DCM.

Supplementary Material

Refer to Web version on PubMed Central for supplementary material.

Acknowledgments

FUNDINGS

This work was supported in part by Grants from the National Science Foundation of China (81370318, to Y.Z.; 81570338, to Z.Z.; 81302860, to Q.L.; 81200917, to X.D.; 81573493, to Q.T.), the Jilin Province Science and Technology Development Project (20130206021SF to J.S.), the Scholarship of China Scholarship Council (201508330753 to L.Q.), the American Diabetes Association (1-15-BS-018 to L.C.), and the National Institute of Health (AA021434, AA024337, and AA020265 to S.-Y.C).

References

1. International Diabetes Federation. IDF Diabetes ATLAS. 7. Brussels: Karakas Print; 2015.
2. Avogaro A, Vigili de Kreutzenberg S, Negut C, Tiengo A, Scognamiglio R. Diabetic cardiomyopathy: a metabolic perspective. Am J Cardiol. 2004; 93:13a–16a.
3. Yilmaz S, Canpolat U, Aydogdu S, Abboud HE. Diabetic Cardiomyopathy; Summary of 41 Years. Korean Circ J. 2015; 45:266–272. [PubMed: 26240579]
4. Kajstura J, Fiordaliso F, Andreoli AM, Li B, Chimenti S, Medow MS, Limana F, Nadal-Ginard B, Leri A, Anversa P. IGF-1 overexpression inhibits the development of diabetic cardiomyopathy and angiotensin II-mediated oxidative stress. Diabetes. 2001; 50:1414–1424. [PubMed: 11375343]
5. Van Linthout S, Seeland U, Riad A, Eckhardt O, Hohl M, Dhayat N, Richter U, Fischer JW, Bohm M, Pauschinger M, et al. Reduced MMP-2 activity contributes to cardiac fibrosis in experimental diabetic cardiomyopathy. Basic Res Cardiol. 2008; 103:319–327. [PubMed: 18347835]
6. Shiomi T, Tsutsui H, Ikeuchi M, Matsusaka H, Hayashidani S, Suematsu N, Wen J, Kubota T, Takeshita A. Streptozotocin-induced hyperglycemia exacerbates left ventricular remodeling and

failure after experimental myocardial infarction. J Am Coll Cardiol. 2003; 42:165–172. [PubMed: 12849678]

7. Boudina S, Abel ED. Diabetic cardiomyopathy revisited. Circulation. 2007; 115:3213–3223. [PubMed: 17592090]
8. Monkemann H, De Vriese AS, Blom HJ, Kluijtmans LA, Heil SG, Schild HH, Golubnitschaja O. Early molecular events in the development of the diabetic cardiomyopathy. Amino Acids. 2002; 23:331–336. [PubMed: 12373555]
9. Cai L, Kang YJ. Oxidative stress and diabetic cardiomyopathy: a brief review. Cardiovasc Toxicol. 2001; 1:181–193. [PubMed: 12213971]
10. Cooper ME. Metabolic memory: implications for diabetic vascular complications. Pediatr Diabetes. 2009; 10:343–346. [PubMed: 19490497]
11. Intine RV, Sarras MP Jr. Metabolic memory and chronic diabetes complications: potential role for epigenetic mechanisms. Curr Diab Rep. 2012; 12:551–559. [PubMed: 22760445]
12. Reddy MA, Zhang E, Natarajan R. Epigenetic mechanisms in diabetic complications and metabolic memory. Diabetologia. 2015; 58:443–455. [PubMed: 25481708]
13. Gregoretti IV, Lee YM, Goodson HV. Molecular evolution of the histone deacetylase family: functional implications of phylogenetic analysis. J Mol Biol. 2004; 338:17–31. [PubMed: 15050820]
14. Lee TI, Kao YH. HDAC Inhibition Modulates Cardiac PPARs and Fatty Acid Metabolism in Diabetic Cardiomyopathy. PPAR Res. 2016; 2016:5938740. [PubMed: 27446205]
15. Chen Y, Du J, Zhao YT, Zhang L, Lv G, Zhuang S, Qin G, Zhao TC. Histone deacetylase (HDAC) inhibition improves myocardial function and prevents cardiac remodeling in diabetic mice. Cardiovasc Diabetol. 2015; 14:99. [PubMed: 26245924]
16. Tan Y, Ichikawa T, Li J, Si Q, Yang H, Chen X, Goldblatt CS, Meyer CJ, Li X, Cai L, et al. Diabetic downregulation of Nrf2 activity via ERK contributes to oxidative stress-induced insulin resistance in cardiac cells in vitro and in vivo. Diabetes. 2011; 60:625–633. [PubMed: 21270272]
17. Wu H, Li GN, Xie J, Li R, Chen QH, Chen JZ, Wei ZH, Kang LN, Xu B. Resveratrol ameliorates myocardial fibrosis by inhibiting ROS/ERK/TGF-beta/periostin pathway in STZ-induced diabetic mice. BMC Cardiovasc Disord. 2016; 16:5. [PubMed: 26750922]
18. Ferguson BS, Harrison BC, Jeong MY, Reid BG, Wempe MF, Wagner FF, Holson EB, McKinsey TA. Signal-dependent repression of DUSP5 by class I HDACs controls nuclear ERK activity and cardiomyocyte hypertrophy. Proc Natl Acad Sci U S A. 2013; 110:9806–9811. [PubMed: 23720316]
19. Sharifi-Sanjani M, Shoushtari AH, Quiroz M, Baust J, Sestito SF, Mosher M, Ross M, McTiernan CF, St Croix CM, Bilonick RA, et al. Cardiac CD47 drives left ventricular heart failure through Ca2+-CaMKII-regulated induction of HDAC3. J Am Heart Assoc. 2014; 3:e000670. [PubMed: 24922625]
20. Samant SA, Pillai VB, Sundaresan NR, Shroff SG, Gupta MP. Histone Deacetylase 3 (HDAC3)-dependent Reversible Lysine Acetylation of Cardiac Myosin Heavy Chain Isoforms Modulates Their Enzymatic and Motor Activity. J Biol Chem. 2015; 290:15559–15569. [PubMed: 25911107]
21. Montgomery RL, Potthoff MJ, Haberland M, Qi X, Matsuzaki S, Humphries KM, Richardson JA, Bassel-Duby R, Olson EN. Maintenance of cardiac energy metabolism by histone deacetylase 3 in mice. J Clin Invest. 2008; 118:3588–3597. [PubMed: 18830415]
22. Juengel E, Makarevic J, Tsaur I, Bartsch G, Nelson K, Haferkamp A, Blaheta RA. Resistance after chronic application of the HDAC-inhibitor valproic acid is associated with elevated Akt activation in renal cell carcinoma in vivo. PLoS One. 2013; 8:e53100. [PubMed: 23372654]
23. Xu Z, Wang S, Ji H, Zhang Z, Chen J, Tan Y, Wintergerst K, Zheng Y, Sun J, Cai L. Broccoli sprout extract prevents diabetic cardiomyopathy via Nrf2 activation in db/db T2DM mice. Sci Rep. 2016; 6:30252. [PubMed: 27457280]
24. Jiang X, Zhang C, Xin Y, Huang Z, Tan Y, Huang Y, Wang Y, Feng W, Li X, Li W, et al. Protective effect of FGF21 on type 1 diabetes-induced testicular apoptotic cell death probably via both mitochondrial- and endoplasmic reticulum stress-dependent pathways in the mouse model. Toxicol Lett. 2013; 219:65–76. [PubMed: 23499715]

25. Wang Y, Wang Y, Luo M, Wu H, Kong L, Xin Y, Cui W, Zhao Y, Wang J, Liang G, et al. Novel curcumin analog C66 prevents diabetic nephropathy via JNK pathway with the involvement of p300/CBP-mediated histone acetylation. Biochim Biophys Acta. 2015; 1852:34–46. [PubMed: 25446993]
26. Greenbaum CJ. Insulin resistance in type 1 diabetes. Diabetes Metab Res Rev. 2002; 18:192–200. [PubMed: 12112937]
27. Manna P, Achari AE, Jain SK. Vitamin D supplementation inhibits oxidative stress and upregulate SIRT1/AMPK/GLUT4 cascade in high glucose-treated 3T3L1 adipocytes and in adipose tissue of high fat diet-fed diabetic mice. Arch Biochem Biophys. 2017; 615:22–34. [PubMed: 28063949]
28. Wang S, Ding L, Ji H, Xu Z, Liu Q, Zheng Y. The Role of p38 MAPK in the Development of Diabetic Cardiomyopathy. Int J Mol Sci. 2016; 17
29. Mandl M, Slack DN, Keyse SM. Specific inactivation and nuclear anchoring of extracellular signal-regulated kinase 2 by the inducible dual-specificity protein phosphatase DUSP5. Mol Cell Biol. 2005; 25:1830–1845. [PubMed: 15713638]
30. Choudhary C, Kumar C, Gnad F, Nielsen ML, Rehman M, Walther TC, Olsen JV, Mann M. Lysine acetylation targets protein complexes and co-regulates major cellular functions. Science. 2009; 325:834–840. [PubMed: 19608861]
31. Lundby A, Lage K, Weinert BT, Bekker-Jensen DB, Secher A, Skovgaard T, Kelstrup CD, Dmytriyev A, Choudhary C, Lundby C, et al. Proteomic analysis of lysine acetylation sites in rat tissues reveals organ specificity and subcellular patterns. Cell Rep. 2012; 2:419–431. [PubMed: 22902405]
32. Ooi JY, Tuano NK, Rafehi H, Gao XM, Ziemann M, Du XJ, El-Osta A. HDAC inhibition attenuates cardiac hypertrophy by acetylation and deacetylation of target genes. Epigenetics. 2015; 10:418–430. [PubMed: 25941940]
33. Morales CR, Li DL, Pedrozo Z, May HI, Jiang N, Kyrychenko V, Cho GW, Kim SY, Wang ZV, Rotter D, et al. Inhibition of class I histone deacetylases blunts cardiac hypertrophy through TSC2-dependent mTOR repression. Sci Signal. 2016; 9:ra34. [PubMed: 27048565]
34. Nural-Guvener H, Zakharova L, Feehery L, Sljukic S, Gaballa M. Anti-Fibrotic Effects of Class I HDAC Inhibitor, Mocetinostat Is Associated with IL-6/Stat3 Signaling in Ischemic Heart Failure. Int J Mol Sci. 2015; 16:11482–11499. [PubMed: 25997003]
35. Nural-Guvener HF, Zakharova L, Nimlos J, Popovic S, Mastroeni D, Gaballa MA. HDAC class I inhibitor, Mocetinostat, reverses cardiac fibrosis in heart failure and diminishes CD90+ cardiac myofibroblast activation. Fibrogenesis Tissue Repair. 2014; 7:10. [PubMed: 25024745]
36. Cardinale JP, Sriramula S, Pariaut R, Guggilam A, Mariappan N, Elks CM, Francis J. HDAC inhibition attenuates inflammatory, hypertrophic, and hypertensive responses in spontaneously hypertensive rats. Hypertension. 2010; 56:437–444. [PubMed: 20679181]
37. Lkhagva B, Lin YK, Kao YH, Chazo TF, Chung CC, Chen SA, Chen YJ. Novel Histone Deacetylase Inhibitor Modulates Cardiac Peroxisome Proliferator-Activated Receptors and Inflammatory Cytokines in Heart Failure. Pharmacology. 2015; 96:184–191. [PubMed: 26304494]
38. McKinsey TA. Targeting inflammation in heart failure with histone deacetylase inhibitors. Mol Med. 2011; 17:434–441. [PubMed: 21267510]
39. Zhou L, He X, Gao B, Xiong S. Inhibition of Histone Deacetylase Activity Aggravates Coxsackievirus B3-Induced Myocarditis by Promoting Viral Replication and Myocardial Apoptosis. J Virol. 2015; 89:10512–10523. [PubMed: 26269170]
40. Rumbaugh G, Sillivan SE, Ozkan ED, Rojas CS, Hubbs CR, Aceti M, Kilgore M, Kudugunti S, Puthanveettil SV, Sweatt JD, et al. Pharmacological Selectivity Within Class I Histone Deacetylases Predicts Effects on Synaptic Function and Memory Rescue. Neuropsychopharmacology. 2015; 40:2307–2316. [PubMed: 25837283]
41. Steliou K, Boosalis MS, Perrine SP, Sangerman J, Faller DV. Butyrate histone deacetylase inhibitors. Biores Open Access. 2012; 1:192–198. [PubMed: 23514803]
42. Kim SW, Hooker JM, Otto N, Win K, Muench L, Shea C, Carter P, King P, Reid AE, Volkow ND, et al. Whole-body pharmacokinetics of HDAC inhibitor drugs, butyric acid, valproic acid and 4-phenylbutyric acid measured with carbon-11 labeled analogs by PET. Nucl Med Biol. 2013; 40:912–918. [PubMed: 23906667]

43. Catalano MG, Pugliese M, Gallo M, Brignardello E, Milla P, Orlandi F, Limone PP, Arvat E, Boccuzzi G, Piovesan A. Valproic Acid, a Histone Deacetylase Inhibitor, in Combination with Paclitaxel for Anaplastic Thyroid Cancer: Results of a Multicenter Randomized Controlled Phase II/III Trial. Int J Endocrinol. 2016; 2016:2930414. [PubMed: 27766105]
44. Caponigro F, Di Gennaro E, Ionna F, Longo F, Aversa C, Pavone E, Maglione MG, Di Marzo M, Muto P, Cavalcanti E, et al. Phase II clinical study of valproic acid plus cisplatin and cetuximab in recurrent and/or metastatic squamous cell carcinoma of Head and Neck-V-CHANCE trial. 2016; 16:918.
45. Olsen KB, Tauboll E, Gjerstad L. Valproate is an effective, well-tolerated drug for treatment of status epilepticus/serial attacks in adults. Acta Neurol Scand Suppl. 2007; 187:51–54. [PubMed: 17419829]
46. Lee TM, Lin MS, Chang NC. Inhibition of histone deacetylase on ventricular remodeling in infarcted rats. Am J Physiol Heart Circ Physiol. 2007; 293:H968–977. [PubMed: 17400721]
47. Cho YK, Eom GH, Kee HJ, Kim HS, Choi WY, Nam KI, Ma JS, Kook H. Sodium valproate, a histone deacetylase inhibitor, but not captopril, prevents right ventricular hypertrophy in rats. Circ J. 2010; 74:760–770. [PubMed: 20208383]
48. Kee HJ, Bae EH, Park S, Lee KE, Suh SH, Kim SW, Jeong MH. HDAC inhibition suppresses cardiac hypertrophy and fibrosis in DOCA-salt hypertensive rats via regulation of HDAC6/HDAC8 enzyme activity. Kidney Blood Press Res. 2013; 37:229–239. [PubMed: 23868068]
49. Patel BM, Raghunathan S, Porwal U. Cardioprotective effects of magnesium valproate in type 2 diabetes mellitus. Eur J Pharmacol. 2014; 728:128–134. [PubMed: 24530414]
50. Barter MJ, Pybus L, Litherland GJ, Rowan AD, Clark IM, Edwards DR, Cawston TE, Young DA. HDAC-mediated control of ERK- and PI3K-dependent TGF-beta-induced extracellular matrix-regulating genes. Matrix Biol. 2010; 29:602–612. [PubMed: 20470885]
51. Lorenz K, Schmitt JP, Schmitteckert EM, Lohse MJ. A new type of ERK1/2 autophosphorylation causes cardiac hypertrophy. Nat Med. 2009; 15:75–83. [PubMed: 19060905]
52. Vidal M, Wieland T, Lohse MJ, Lorenz K. beta-Adrenergic receptor stimulation causes cardiac hypertrophy via a Gbetagamma/Erk-dependent pathway. Cardiovasc Res. 2012; 96:255–264. [PubMed: 22843704]
53. Xu W, Wu W, Chen J, Guo R, Lin J, Liao X, Feng J. Exogenous hydrogen sulfide protects H9c2 cardiac cells against high glucose-induced injury by inhibiting the activities of the p38 MAPK and ERK1/2 pathways. Int J Mol Med. 2013; 32:917–925. [PubMed: 23912965]
54. Tan HW, Sim AY, Huang SL, Leng Y, Long YC. HC toxin (a HDAC inhibitor) enhances IRS1-Akt signalling and metabolism in mouse myotubes. J Mol Endocrinol. 2015; 55:197–207. [PubMed: 26373795]
55. Chriett S, Zerzaihi O, Vidal H, Pirola L. The histone deacetylase inhibitor sodium butyrate improves insulin signalling in palmitate-induced insulin resistance in L6 rat muscle cells through epigenetically-mediated up-regulation of Irs1. Mol Cell Endocrinol. 2017; 439:224–232. [PubMed: 27619406]
56. Khan S, Jena GB. Protective role of sodium butyrate, a HDAC inhibitor on beta-cell proliferation, function and glucose homeostasis through modulation of p38/ERK MAPK and apoptotic pathways: study in juvenile diabetic rat. Chem Biol Interact. 2014; 213:1–12. [PubMed: 24530320]
57. Zhang L, Du J, Yano N, Wang H, Zhao YT, Patricia DS, Zhuang S, Chin EY, Qin G, Zhao TC. Sodium Butyrate Protects Against High Fat Diet-induced Cardiac Dysfunction and Metabolic Disorders in Type II Diabetic Mice. J Cell Biochem. 2017
58. Lee TI, Kao YH. HDAC Inhibition Modulates Cardiac PPARs and Fatty. Acid Metabolism in Diabetic Cardiomyopathy. 2016; 2016:5938740.
59. Epstein PN, Overbeek PA, Means AR. Calmodulin-induced early-onset diabetes in transgenic mice. Cell. 1989; 58:1067–1073. [PubMed: 2673540]
60. Avery LB, Bumpus NN. Valproic acid is a novel activator of AMP-activated protein kinase and decreases liver mass, hepatic fat accumulation, and serum glucose in obese mice. Mol Pharmacol. 2014; 85:1–10. [PubMed: 24105977]

Abbreviations

3-NT	3-nitrotyrosine
4-HNE	4-hydroxy-2-nonenal
AMPK	5' AMP-activated protein kinase
ANP	atrial natriuretic peptide
ChIP	chromatin immunoprecipitation
CTGF	connective tissue growth factor
DCM	diabetic cardiomyopathy
DUSP5	dual Specificity Phosphatase 5
EF	ejection fraction
ERK	extracellular signal-regulated kinases
FN-1	fibronectin-1
FS	fractional shortening
GLUT1 and 4	glucose transporter type 1 and 4
HDACs	histone deacetylases
IRS1	insulin receptor substrate 1
JNK	c-Jun N-terminal protein kinase
LV	left ventricular
LV vol; d	LV end diastolic volume
LV vol; s	LV end systolic volume
LV	left ventricular
LVID; d	LV internal diastolic diameter
LVID;s	LV internal systolic diameter
MAPK	mitogen-activated protein kinase
MDA	malondialdehyde
PAI-1	plasminogen activator inhibitor-1
ROS	reactive oxygen species
STZ	streptozotocin
TNF-α	tumor necrosis factor alpha

VPA	valproic acid
WGA	wheat germ agglutinin
WT	wild-type

CLINICAL PERSPECTIVES

- Although a few studies showed the association of total HDAC inhibition with DCM, we are the first to specifically define the pivotal role of HDAC3 inhibition in preventing DCM
- HDAC3 inhibition prevents type 1 diabetes-induced cardiac inflammation, remodeling, and dysfunction, which reaches to the same effect of total HADC inhibition. The cardiac protection by HDAC3 inhibition from DCM is persistent even until 3 months after the end of treatment, like a phenomenon of “protective memory”. Mechanistically, the cardioprotection of HDAC3 inhibition is likely mediated by the epigenetic regulation of DUSP5-ERK1/2 pathway via acetylating of histone H3 on the DUSP5 gene promoter.
- This study suggests that HDAC3 may be an important target potentially for clinical application to prevent DCM in type 1 diabetic patients.

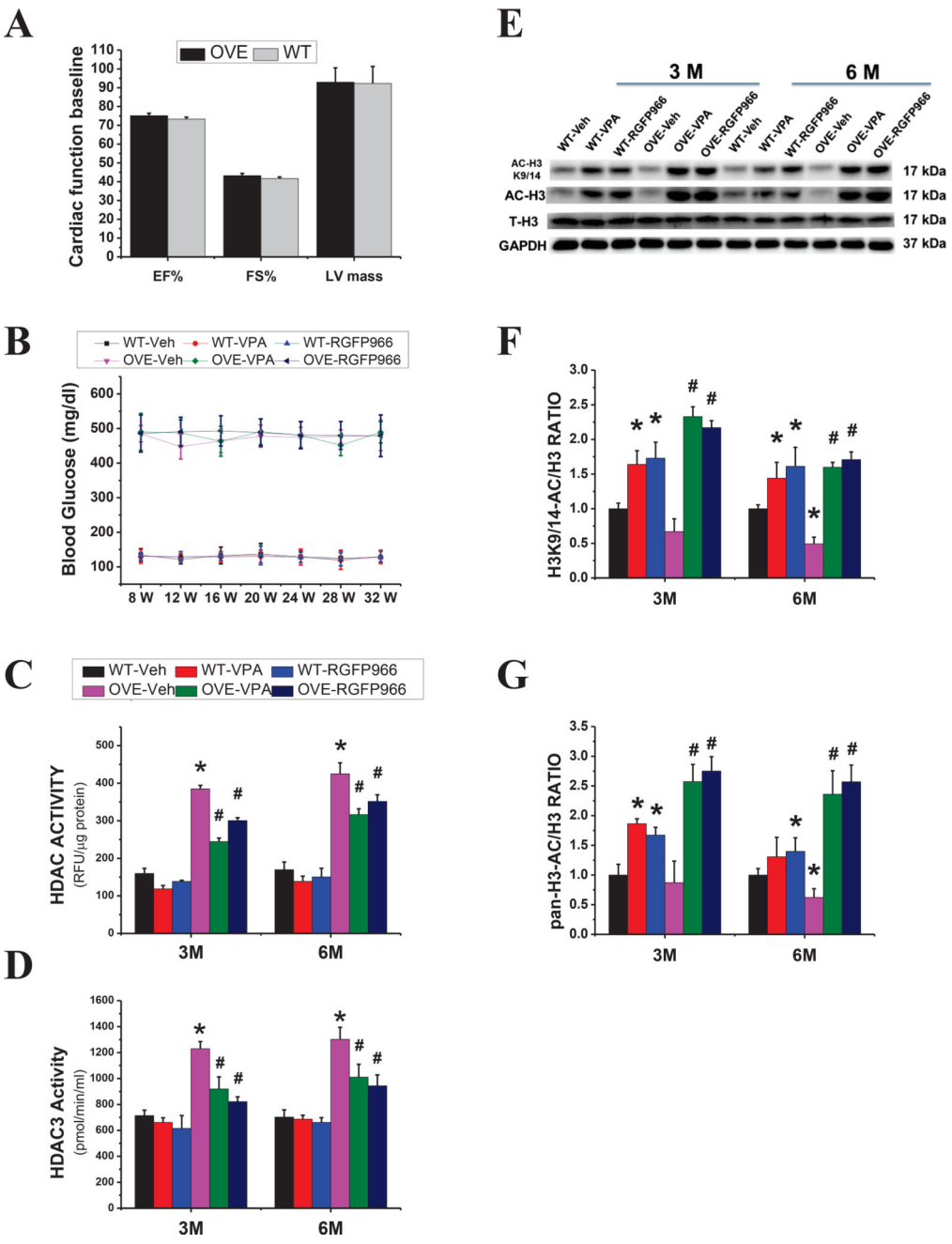

Figure 1. General feature of mice and effects of VPA and RGFP966 on HDAC and HDAC3 activity

The main cardiac function parameters before treatment of HDAC inhibitor (A) and the time course of blood glucose levels (B) in both OVE26 and WT mice. Measurement of HDAC and HDAC3 activity in the diabetic heart from different groups as indicated (C, D). Representative results and densitometric analyses of Western blot of AC-H3, ACH3K9/14 (E–G). Data are presented as the mean ± S.D. n=5–7 per group. $^{*}P < 0.05$ vs. WT-Veh; $^{\#}P < 0.05$ vs. OVE-Veh at the same time point.

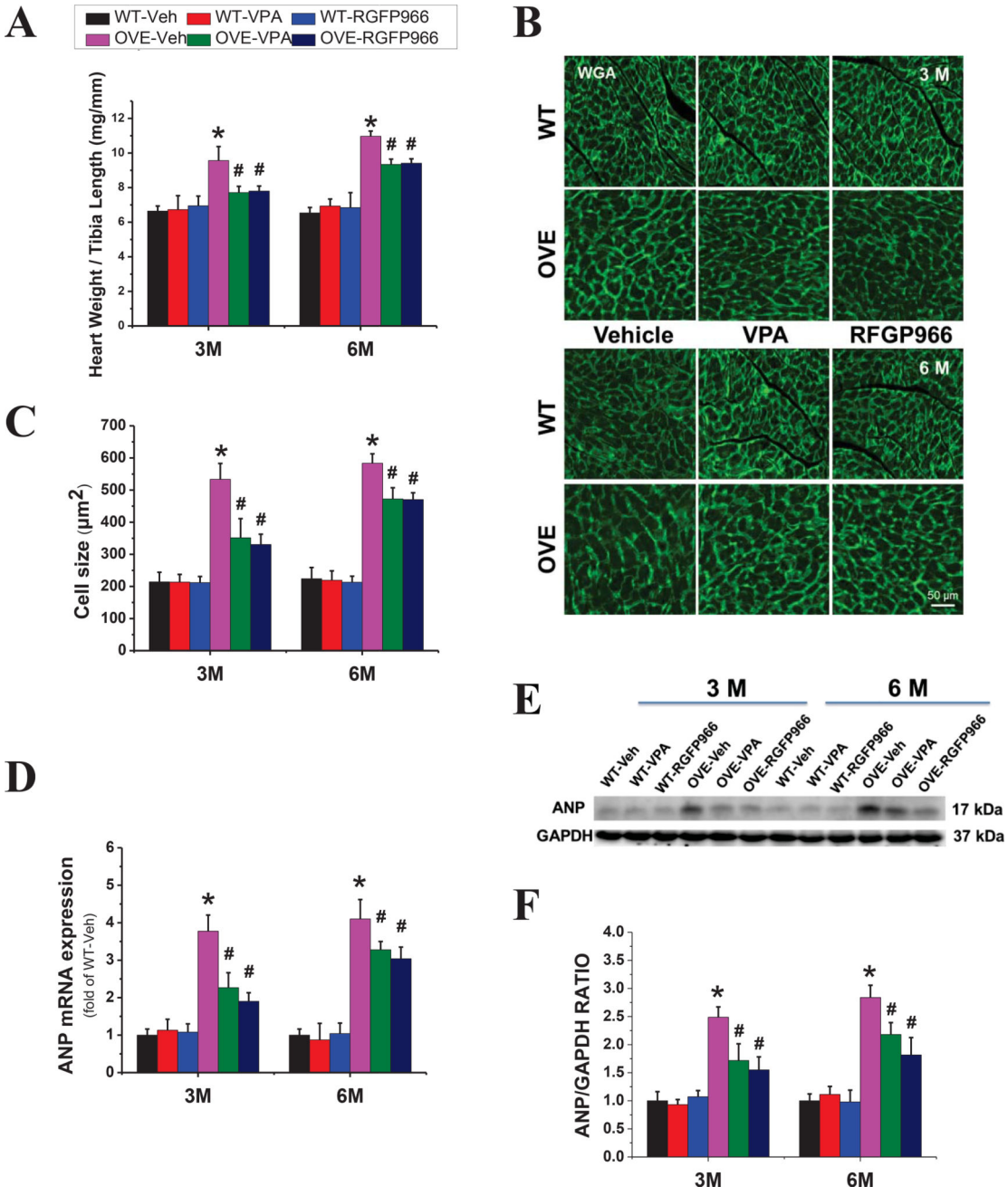

Figure 2. RGFP966 prevented diabetes-induced cardiac hypertrophy

The ratio of heart weight to tibia length (A). Representative images of cardiac tissue FITC-conjugated WGA staining in the animal hearts and quantification of myocyte cross-sectional areas (B, C). The expression of cardiac hypertrophic marker ANP detected at the levels of mRNA (B) and protein (D) by real-time PCR and Western blot (E, F), respectively. Data are presented as the mean ± S.D. n=5–7. **P* < 0.05 vs. WT-Veh; #*P* < 0.05 vs. OVE-Veh at the same time point.

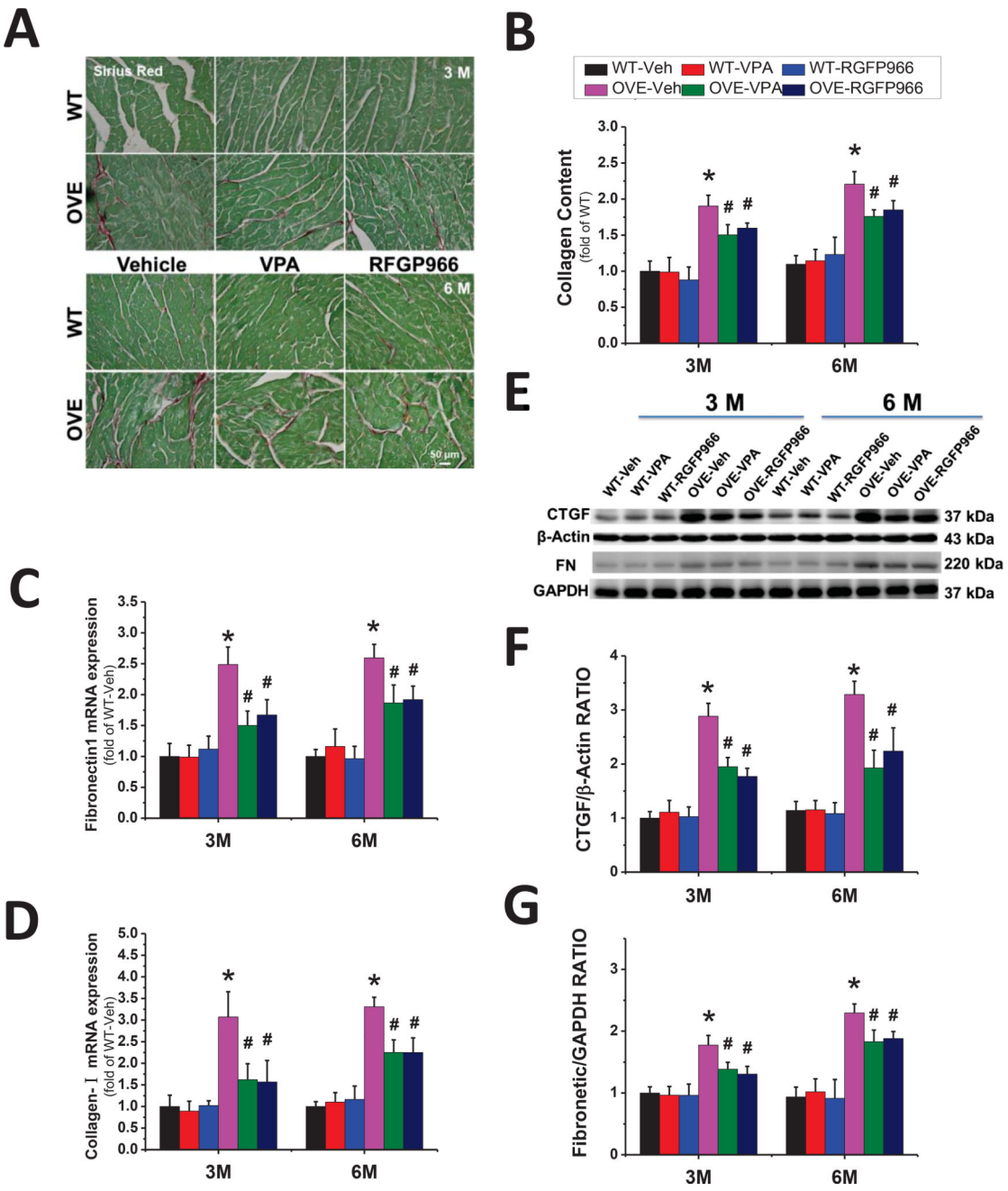

Figure 3. RGFP966 prevented diabetes-induced cardiac fibrosis

Representative images of Sirius red staining and quantification of collagen content (A, B). Real-time PCR for transcription of collagen I (C) and FN-1 (D). Representative results and densitometric analyses of Western blot for CTGF and FN-1 in the heart (E–G). Data are presented as the mean ± S.D. n=5–7. **P* < 0.05 vs. WT-Veh; #*P* < 0.05 vs. OVE-Veh at the same time point.

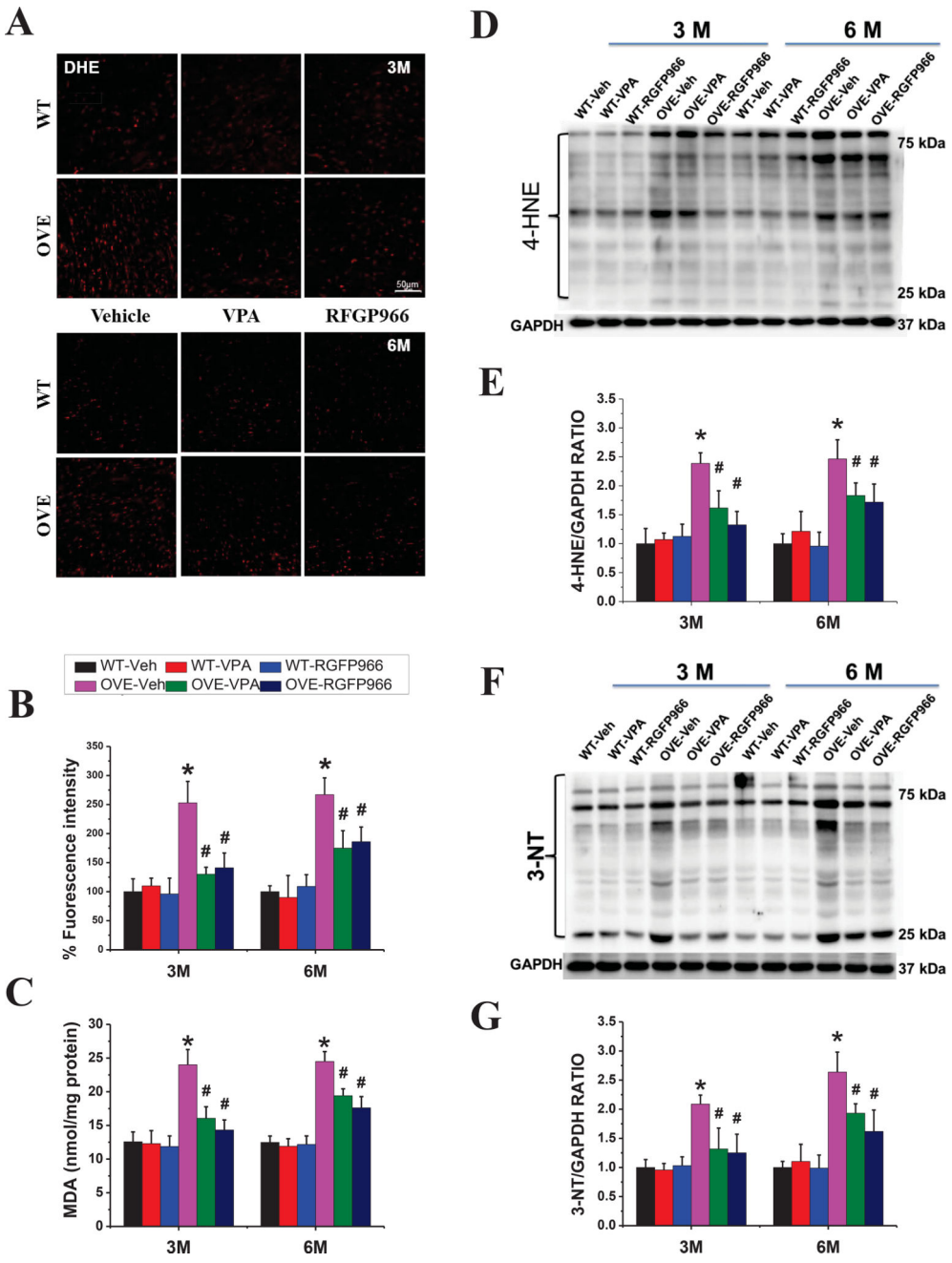

Figure 4. RGFP966 prevented diabetes-induced cardiac oxidative stress

Representative images of DHE staining and quantification of fluorescence intensity (A, B). Lipid peroxide accumulation quantified by MDA (C). Representative results and densitometric analyses of Western blot for 4-HNE and 3-NT protein (D–G). Data are presented as the mean ± S.D. n=5–7. *$P < 0.05$ vs. WT-Veh; #$P < 0.05$ vs. OVE-Veh at the same time point.

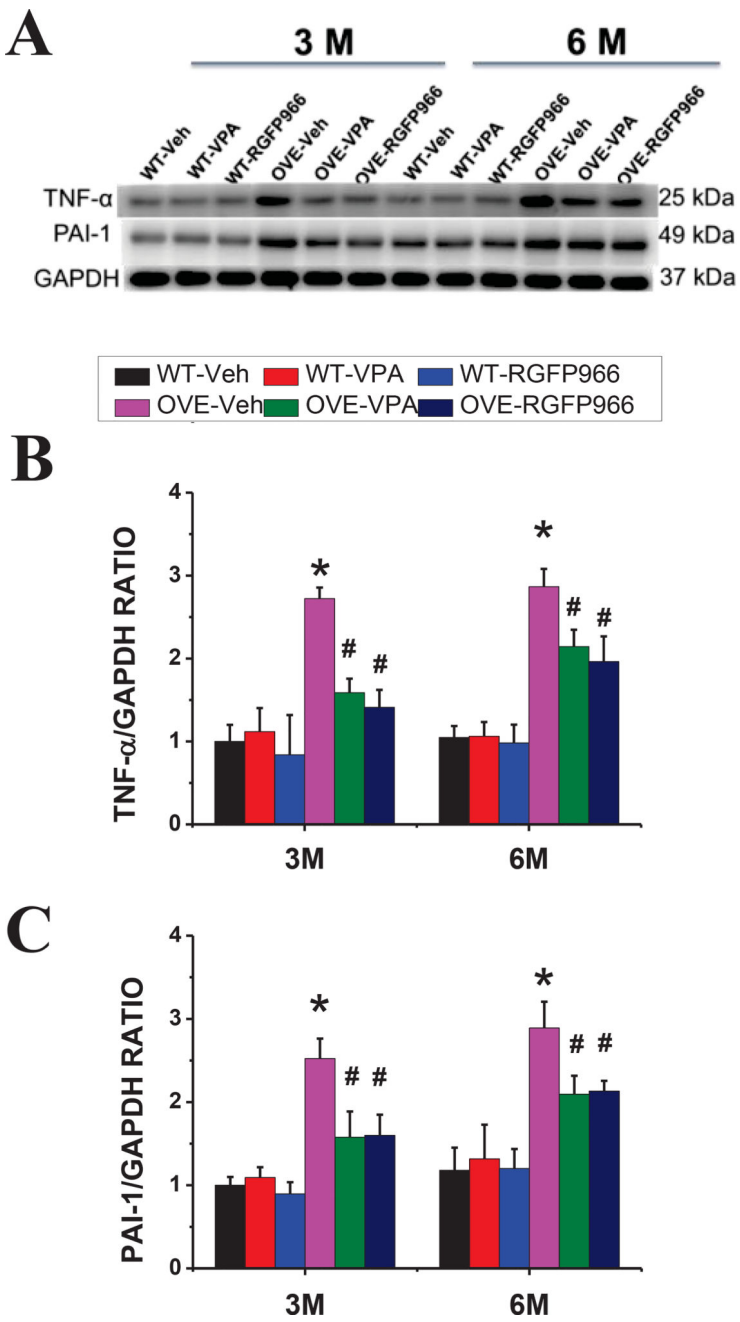

Figure 5. RGFP966 prevented diabetes-induced cardiac inflammation

Representative result and densitometric analyses of Western blot of PAI-1 and TNF-α proteins (A–C). Data are presented as the mean ± S.D. n=5–7. **P* < 0.05 vs. WT-Veh; #*P* < 0.05 vs. OVE-Veh at the same time point.

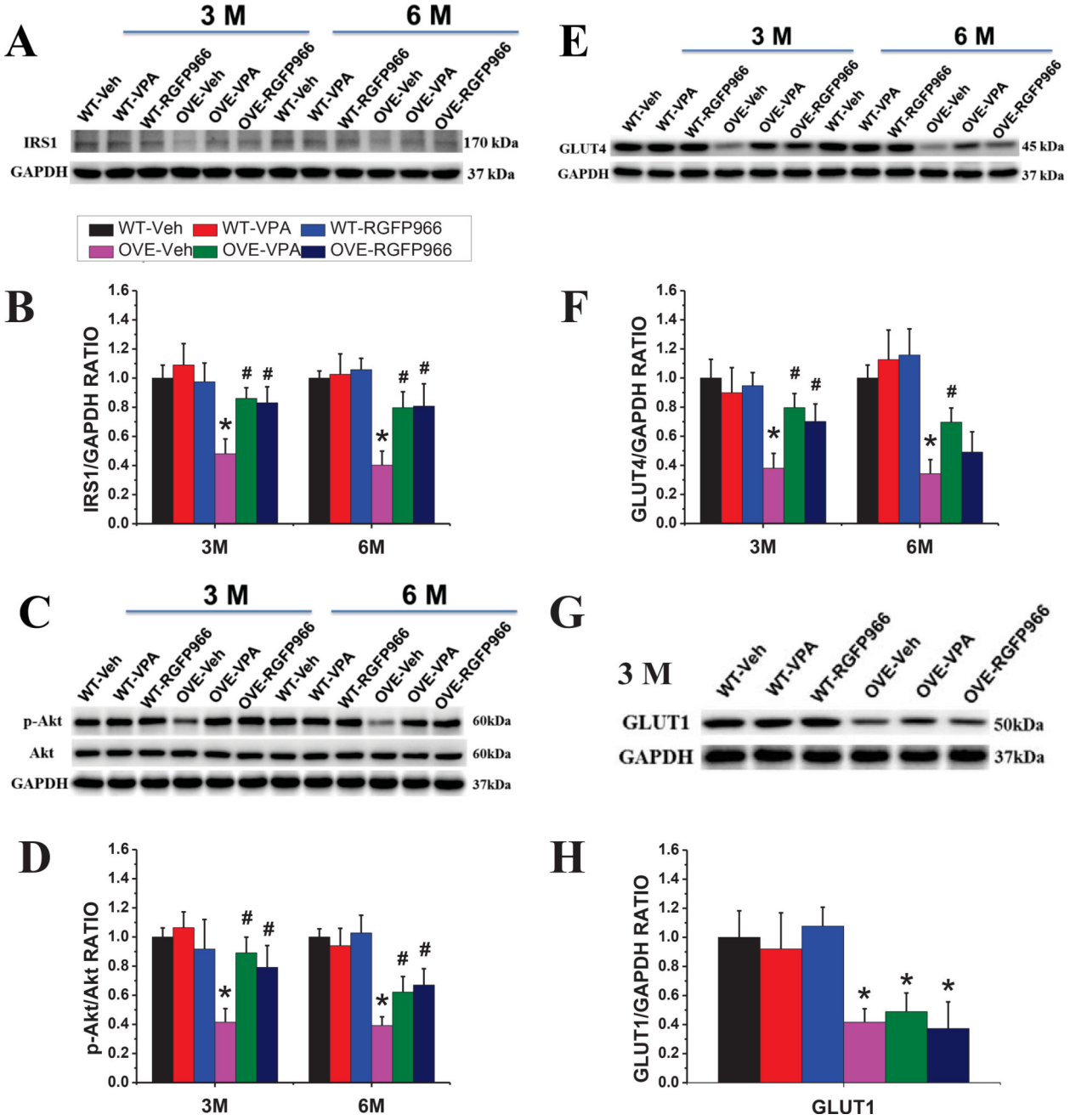

Figure 6. RGFP966 improved insulin receptor signaling pathway in the OVE26 mouse heart

Representative results of Western blot for IRS1, Akt, GLUT4, and GLUT1 protein (A, C, E, G). Densitometric analyses of Western blot for IRS1, Akt, GLUT4 and GLUT1 (B, D, F, H). Data are presented as the mean ± S.D. n=5–7. *P < 0.05 vs. WT-Veh; #P < 0.05 vs. OVE-Veh at the same time point.

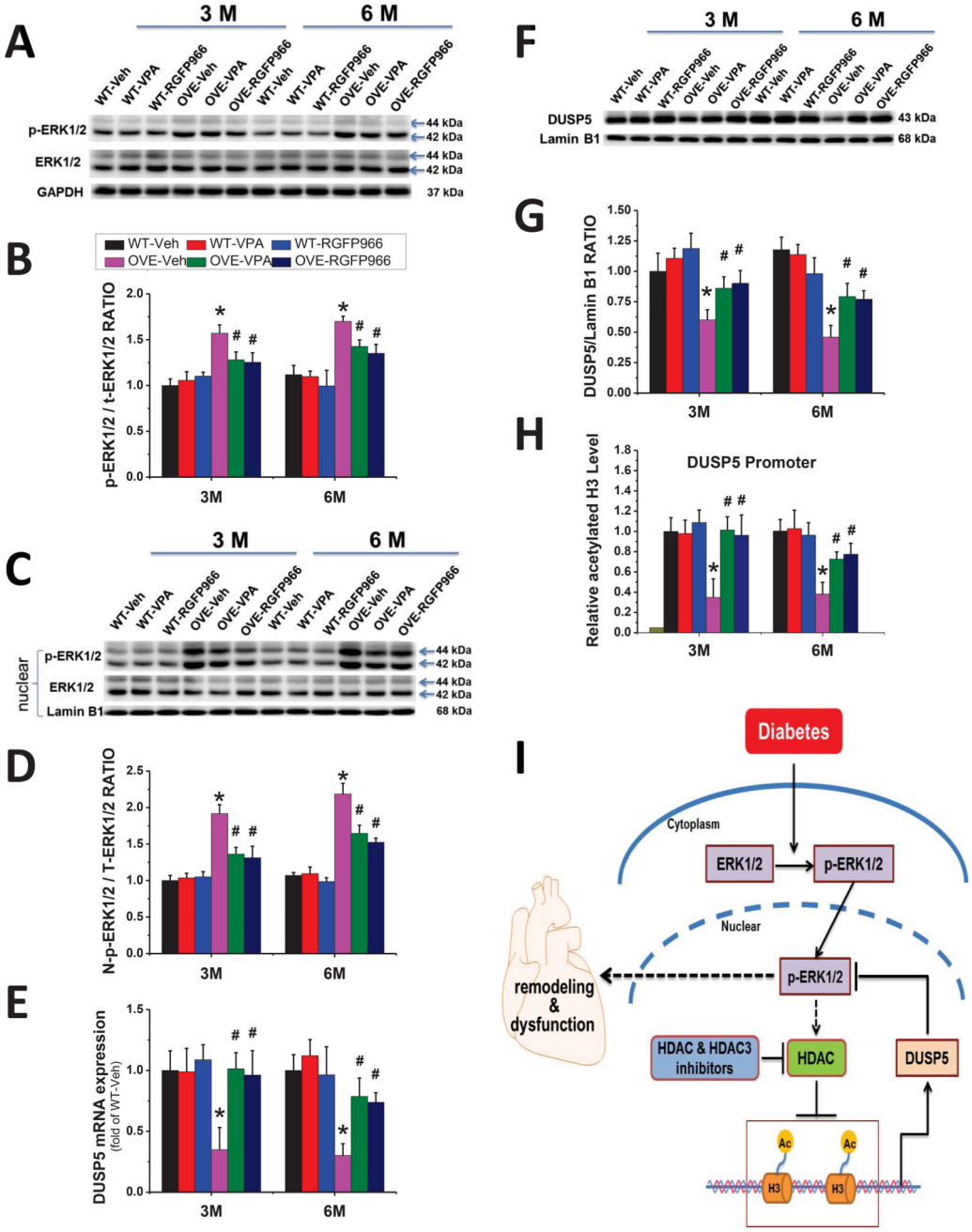

Figure 7. RGFP966 blocked the activation of cardiac ERK1/2 in the nucleus by epigenetic regulation of DUSP5 via histone H3 acetylation

Representative Western blot of whole cell p-ERK1/2 and ERK1/2, nuclear p-ERK1/2 and ERK1/2 (A, C), and densitometric analyses of Western blot of p-ERK1/2 protein levels (B, D). The expression of DUSP5 detected by real-time PCR (E) and Western blot (F, G). The acetylated level of histone H3 on the DUSP5 gene promoter region revealed by ChIP (H). Normal mouse IgG was used as a negative control and data were normalized to input DNA samples. Data are presented as the mean ± S.D. n=5–7. $^{*}P < 0.05$ vs. WT-Veh; $^{\#}P < 0.05$ vs. OVE-Veh at the same time point. Schematic illustration of the working hypothesis for the regulation of nuclear ERK1/2 signaling and diabetes-induced cardiac injury by HDAC3 and

DUSP5 (I). Diabetes increased ERK1/2 phosphorylation and nuclear accumulation of phosphorylated ERK1/2 where it turns on the cardiac apoptosis, hypertrophy and fibrosis signaling pathways, leading to the final cardiac remodeling and dysfunction. HDAC3 (or HDACs) inhibitor stimulates DUSP5 expression by increasing the acetylated histone H3, leading to the dephosphorylation of nuclear ERK1/2 and thus reducing cardiac remodeling and dysfunction. In addition, phosphorylated ERK1/2 also inhibits DUSP5 expression via stimulating HDACs, making a self-reinforcing cycle.

Table 1

Protective effect of VPA and RGFP966 on diabetes-induced cardiac dysfunction.

	WT-Veh	WT-VPA	WT-RGFP966	OVE-Veh	OVE-VPA	OVE-RGFP966
3 M						
IVS;d(mm)	0.63 ± 0.01	0.65 ± 0.03	0.63 ± 0.01	0.62 ± 0.03	0.65 ± 0.02	0.63 ± 0.02
LVID;d(mm)	3.82 ± 0.02	3.86 ± 0.07	3.81 ± 0.02	4.10 ± 0.05 *	3.80 ± 0.02 #	3.81 ± 0.06 #
LVPW;d(mm)	0.85 ± 0.03	0.87 ± 0.03	0.85 ± 0.03	0.80 ± 0.08	0.85 ± 0.03	0.85 ± 0.03
IVS;s(mm)	1.05 ± 0.02	1.03 ± 0.05	1.00 ± 0.04	1.00 ± 0.06	1.06 ± 0.02	1.03 ± 0.02
LVID;s(mm)	2.16 ± 0.02	2.15 ± 0.08	2.18 ± 0.04	2.70 ± 0.09 *	2.13 ± 0.03 #	2.15 ± 0.06 #
LVPW;s(mm)	1.29 ± 0.03	1.30 ± 0.02	1.31 ± 0.02	1.27 ± 0.03	1.28 ± 0.03	1.28 ± 0.03
LV Vol;d(mm)	62.69 ± 0.62	64.34 ± 2.90	62.34 ± 0.62	74.30 ± 2.15 *	63.81 ± 0.80 #	64.42 ± 2.10 #
LV Vol;s(mm)	15.47 ± 0.32	15.34 ± 1.4	15.81 ± 0.76	27.06 ± 2.12 *	15.99 ± 0.61 #	15.39 ± 1.08 #
%EF	75.32 ± 0.24	76.18 ± 1.56	74.64 ± 1.04	63.61 ± 2.24 *	75.74 ± 1.10 #	75.35 ± 1.37 #
%FS	43.43 ± 0.23	44.28 ± 1.43	42.82 ± 0.93	34.18 ± 1.64 *	43.81 ± 1.02 #	43.47 ± 1.24 #
LV Mass(mg)	97.73 ± 2.26	99.62 ± 2.91	96.56 ± 3.75	104.78 ± 2.99 *	97.57 ± 2.59 #	97.93 ± 3.40 #
6 M						
IVS;d(mm)	0.65 ± 0.02	0.65 ± 0.01	0.64 ± 0.01	0.64 ± 0.02	0.62 ± 0.02	0.64 ± 0.02
LVID;d(mm)	3.82 ± 0.07	3.83 ± 0.05	3.77 ± 0.02	4.20 ± 0.12 *	4.02 ± 0.08 *#	3.99 ± 0.03 *#
LVPW;d(mm)	0.87 ± 0.02	0.86 ± 0.01	0.88 ± 0.01	0.91 ± 0.04	0.89 ± 0.06	0.89 ± 0.02
IVS;s(mm)	1.00 ± 0.04	1.03 ± 0.02	1.00 ± 0.05	0.96 ± 0.06	0.95 ± 0.02	0.97 ± 0.04
LVID;s(mm)	2.08 ± 0.00	2.08 ± 0.04	2.06 ± 0.02	2.96 ± 0.09 *	2.48 ± 0.04 *#	2.43 ± 0.02 *#
LVPW;s(mm)	1.30 ± 0.01	1.31 ± 0.01	1.30 ± 0.01	1.33 ± 0.03	1.31 ± 0.04	1.31 ± 0.06
LV Vol;d(mm)	62.55 ± 2.93	63.12 ± 2.30	60.44 ± 0.62	78.94 ± 5.40 *	70.85 ± 3.74 *#	69.68 ± 1.01 *#
LV Vol;s(mm)	14.03 ± 0.30	13.95 ± 0.60	13.72 ± 0.35	34.36 ± 2.58 *	21.92 ± 2.58 *#	20.87 ± 1.00 *#
%EF	77.53 ± 1.11	77.91 ± 0.15	77.00 ± 0.39	56.47 ± 1.75 *	71.93 ± 1.42 *#	71.66 ± 2.09 *#
%FS	45.50 ± 1.12	45.86 ± 0.13	45.20 ± 0.27	29.25 ± 1.17 *	40.64 ± 1.23 *#	40.40 ± 1.78 *#
LV Mass(mg)	99.98 ± 3.42	100.68 ± 2.63	101.52 ± 1.79	127.37 ± 6.18 *	108.36 ± 1.30 *#	110.45 ± 2.28 *#

Notes: IVS: interventricular septum; LVID;d: left ventricular internal diastolic diameter; LVID;s: left ventricular internal systolic diameter; LVPW: left ventricular posterior wall; EF: ejection fraction; FS: fractional shortening; LV vol;s: left ventricular end systolic volume; LV vol;d: left ventricular end diastolic volume; LV mass: left ventricular mass.

Clin Sci (Lond). Author manuscript; available in PMC 2018 August 01.

Data are presented as means ± SD.

*, $p<0.05$ vs. WT-Veh group;

#, $p<0.05$ vs. OVE-Veh group